Journal of Microscopy, Vol. 236, Pt 1 2009, pp. 5–10
Received 17 March 2009; accepted 24 May 2009
doi: 10.1111/j.1365-2818.2009.03207.x

An improved method for nanogold *in situ* hybridization visualized with environmental scanning electron microscopy

C.J. EHRHARDT*, R.M. HAYMON*, S.M. SIEVERT† & P.A. HOLDEN‡
**Department of Earth Science, University of California Santa Barbara, Santa Barbara, CA 93106, U.S.A.*
†Biology Department, Woods Hole Oceanographic Institute, Woods Hole, MA 02543, U.S.A.
‡Donald Bren School of Environmental Science and Management, University of California Santa Barbara, Santa Barbara CA 93106, U.S.A.

Introduction

An important goal in geomicrobiology is the identification of microbes associated with specific mineral surfaces. Yet, simultaneously collecting phylogenetic and mineral information remains methodologically challenging. Recently, whole-cell *in situ* hybridization techniques using oligonucleotide rRNA probes bound to nanogold particles have been used to detect microbes with scanning electron microscopy (SEM) for geomicrobiological applications (Gerard *et al.*, 2005; Kenzaka *et al.*, 2005). These techniques rely on backscattered electron images or energy dispersive X-ray spectroscopy to map the presence and distribution of nanogold, and to identify areas of rRNA hybridization within cells and on mineral surfaces.

Although these nanogold hybridization techniques have been successful for pure cultures of *Bacteria* and *Archaea* (Gerard *et al.*, 2005) and for natural microbial communities associated with river sediment particles (Kenzaka *et al.*, 2005) and basalt surfaces (Menez *et al.*, 2007), their application to other metal-rich geomicrobiological systems is problematic. First, metallic substrates and surfaces can obscure detection of nanogold-labelled cells imaged with backscattered electron microscopy (Richards *et al.*, 2001). Second, metallic surfaces can interfere with the hybridization reaction by causing non-specific precipitation of nanogold (Humbel *et al.*, 1995; Weipoltshammer *et al.*, 2000). Because many geomicrobiological systems of interest have a high concentration of metal substrates (i.e. hydrothermal vents, acid mine drainage) a new technique is needed to identify microbes found in these types of environments.

In this work, we present a new nanogold *in situ* hybridization method that increases the concentration of nanogold probes bound to rRNA targets within the cell and makes individual hybridization events directly visible with secondary electron SEM imaging.

Correspondence to: C.J. Ehrhardt. Tel: +1 (805) 893-3718; fax: +1 (805) 893-2314; e-mail: christopher.ehrhardt@gmail.com

Materials and methods

Our *in situ* hybridization technique follows previously published protocols (Gerard *et al.*, 2005; Kenzaka *et al.*, 2005) with two important exceptions. First, to increase permeability of the cell envelope to the diffusion of nanogold, we used more concentrated treatments of proteinase digestion prior to hybridization (0.1 mg mL^{-1} Proteinase K, New England BioLabs, Ipswich, MA, U.S.A.), and conducted all pre-digestion steps at 37°C for 8 min. Second, because metal ions on mineral surfaces may compete with nanogold-DNA probes for gold precipitation during the enhancement step, we increased the concentration of nanogold probe to a 1:400 dilution (Nanogold-Streptavidin, Nanoprobes, Inc., Yaphank, NY, U.S.A.) and the duration of the gold enhancement step (15 min, using GoldEnhance, Nanoprobes, Inc.).

Our modified nanogold hybridization technique was first tested with separate liquid cultures of *Escherichia coli* strain +pMMB67HE and *Pseudomonas aeruginosa* PG201 (Priester *et al.*, 2007). Exponential phase cultures for both organisms were grown in Luria Bertani broth (Sigma, St. Louis, MO, U.S.A.), and harvested after 8 h in a shaking incubator (30°C, 200 rpm). Cells were washed in 1× PBS (Phospate Buffered Saline), fixed in 4% paraformaldehyde (4°C, 3 h) and spotted onto glass slides.

To test the effectiveness of this method for detecting microbes attached to mineral surfaces and in biofilm communities, a small aliquot (~10 μL) of exponential phase *P. aeruginosa* PG201 (Priester *et al.*, 2007) was spiked into Luria Bertani broth (10 mL), mixed with 50 g sterile Accusand (75–150 μm in size; Unimin Corp, New Canaan, CT, U.S.A.) and incubated for 24 h (30°C, 200 rpm). Following incubation, ~1 g of

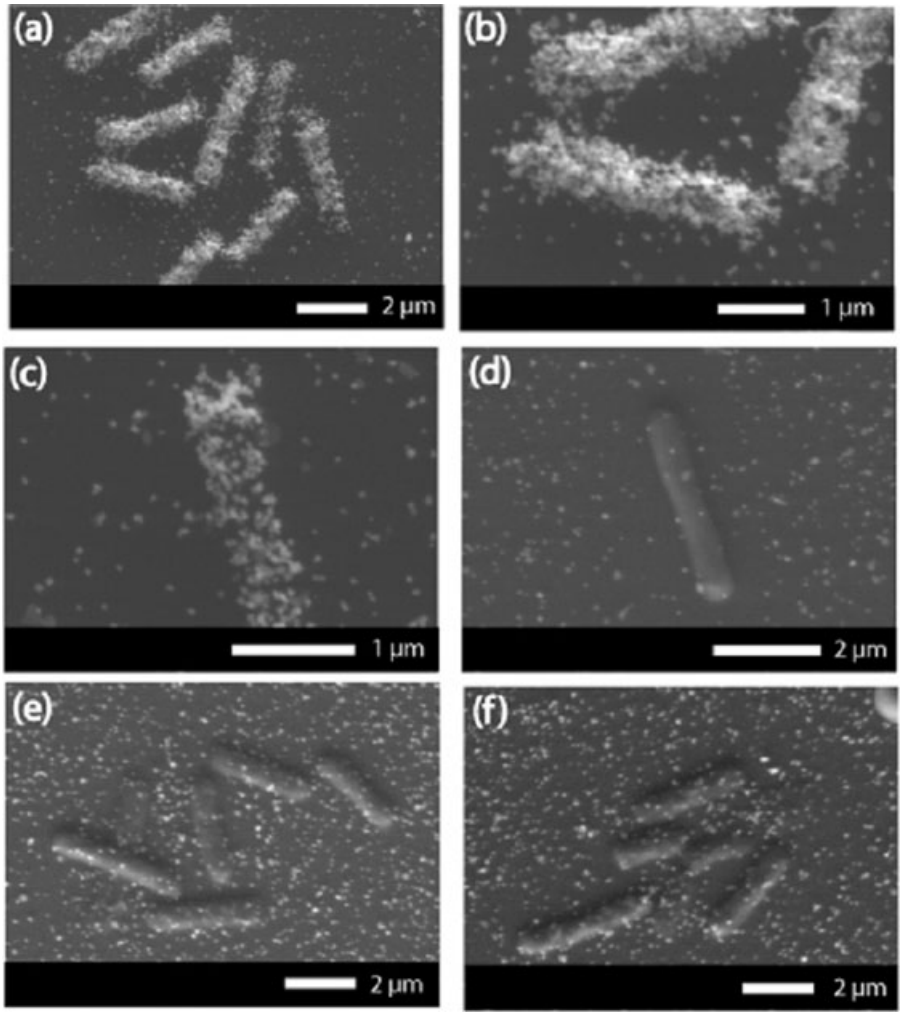

Fig. 1 Secondary-electron ESEM images showing comparison of hybridized and non-hybridized gold probes with *E. coli* cells. Nanogold particles coupled to hybridized bacteria-specific probe fill the volume of the cell, effectively preserving the size and morphology (a and b). Nanogold particle concentration can vary between cells (seen in c and b). Cells hybridized with a negative control probe and coupled to nanogold particles are shown in (d), (e) and (f); each cell is observed only with a few nanogold particles (<10). Particle concentration appears to be the same or less than what is observed on the glass slide surface. For all panels (a–f), E. coli cells were imaged in wet mode (3.9–4.3 torr) with the ESEM without any conductive coating. Cell-specific nanogold binding (a,b,c) exhibits variety values of 21–23; non-specific nanogold binding (d,e,f) exhibits lower average variety values of 11–13.

wet culture slurry was removed, fixed and spotted onto glass slides as before. Both *E. coli* and *P. aeruginosa*-sand cultures were hybridized with *Bacteria*-specific nanogold-rRNA probes EUB338 and NON338 (Delong *et al.*, 1989).

Additionally, we tested the nanogold *in situ* hybridization technique with a hyperthermophilic archaeal culture (*Pyrococcus* GB-D) grown in the presence of microcrystals of pyrite and elemental sulphur (Jannasch *et al.*, 1992) to determine the specificity of hybridization reagents for cells versus metallic mineral surfaces. The culture broth, containing *Pyrococcus* cells, pyrite and sulphur was fixed in 4% paraformaldehyde and spotted onto glass slides as described above. Archaeal specific primer ARC915 (Delong, 1992) was used for nanogold hybridization on these cultures.

All nanogold-hybridized samples were imaged using an FEI Co. XL30 environmental scanning electron microscope (ESEM) (Phillips Electron Optics, Eindhoven, The Netherlands) with a field emission gun operating at either 5 or 15 KeV. Imaging was conducted in both wet mode (3.9–4.4 torr) with a gaseous secondary electron detector or in high vacuum with a secondary electron detector. All samples were air-dried at room temperature prior to imaging. Morphologic and textural differences between nanogold-labelled cells and negative control cells were quantified by variety analysis performed on ESEM images, following methods previously developed (Priester *et al.*, 2007). Variety values were calculated in ArcView 3.2a by using a 6 by 6 pixel kernel because this matches the scale of brightness

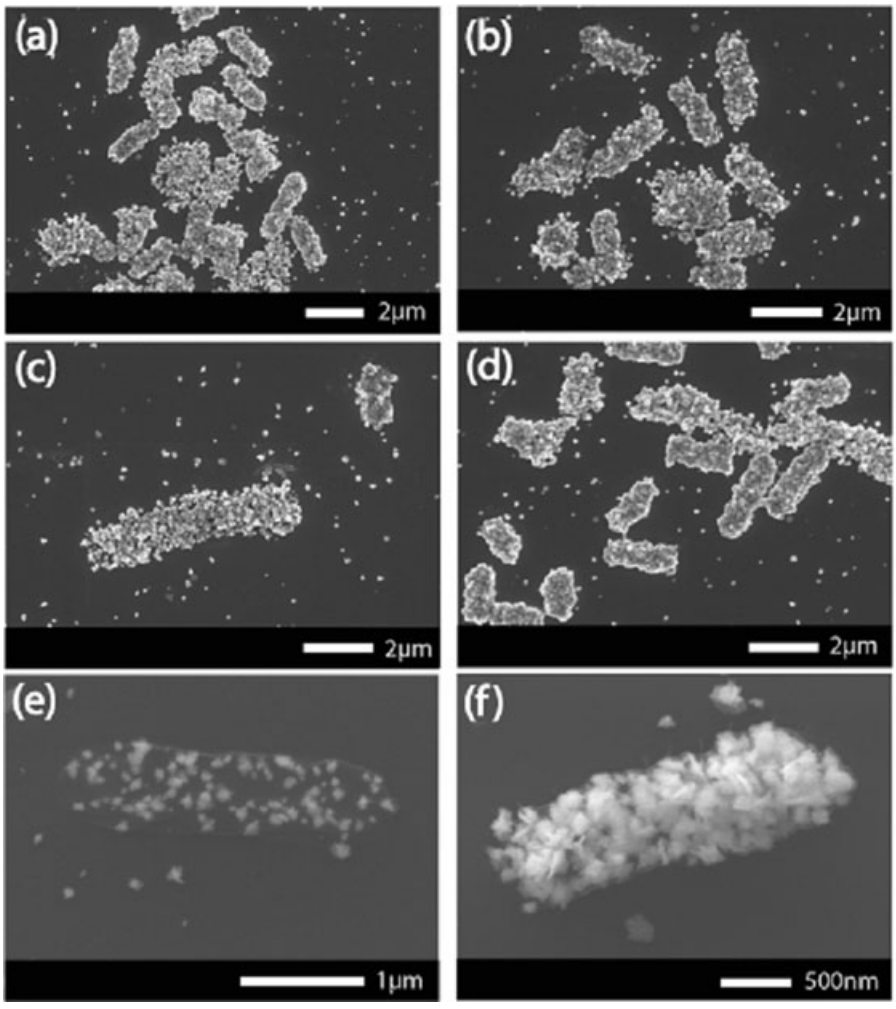

Fig. 2. Nanogold hybridizations with P. aeruginosa pure cultures. P. aeruginosa hybridized to bacteria-specific probe EUB338 were carbon coated and imaged with secondary–electrons in high vacuum mode with the ESEM. A lower accelerating voltage (5 KeV) was used for images in a–d. Small nanogold clusters (20-100nm) hybridize to rRNA molecules within the cell and fill nearly the entire volume of the cell (seen in a–d). Hybridized P. aeruginosa cells were also imaged with higher accelerating beam voltage (15 keV; seen in e and f). Under these conditions, the cell envelope in most specimens is visible (seen in e and f) and serves to restrict probe binding within the cell. As a result, the morphology and size of cells are well preserved and the resulting nanogold precipitates are easily visualized in the field of view. Some variations in binding efficiency are observed between cells as seen in (e) and (f) although this was not prevalent in most experiments performed on pure cultures.

variations seen in hybridization clusters of nanogold particles.

Results and discussion

Results from hybridization experiments on pure cultures of *E. coli* show clusters of nanogold particles (~70–150 nm) arranged in the size and shape of bacterial cells (Fig. 1a–c). The size, morphology and electron density (determined from secondary electron image) of individual bright features are consistent with enhanced nanogold particles. When imaged in wet mode (ca.4 torr), cell envelopes are not visible (Fig. 1a–c). Variations in nanogold concentration within cells are observed (Fig. 1b versus 1c) and nonspecific associations of nanogold particles are also observed on the glass slide around hybridized cells (Fig 1a–c) at apparently lower nanogold concentrations than the areas within cells.

Bacterial cells hybridized to a negative control probe have relatively low numbers of nanogold particles directly associated with the cell (<10; Fig. 1d–f). Cell boundaries are visible and a few (<6) nanogold particles are associated with cell surfaces. *E. coli* cells hybridized with EUB338 nanogold probe (Fig. 1) showed a higher average variety value (22 ± 1, $n = 29$) compared to negative control cells (average variety 12 ± 1, $n = 9$).

Nanogold hybridizations with exponential phase *P. aeruginosa* cells and EUB338 probe show similar results in that enhanced nanogold particle clusters (~70–150 nm) fill

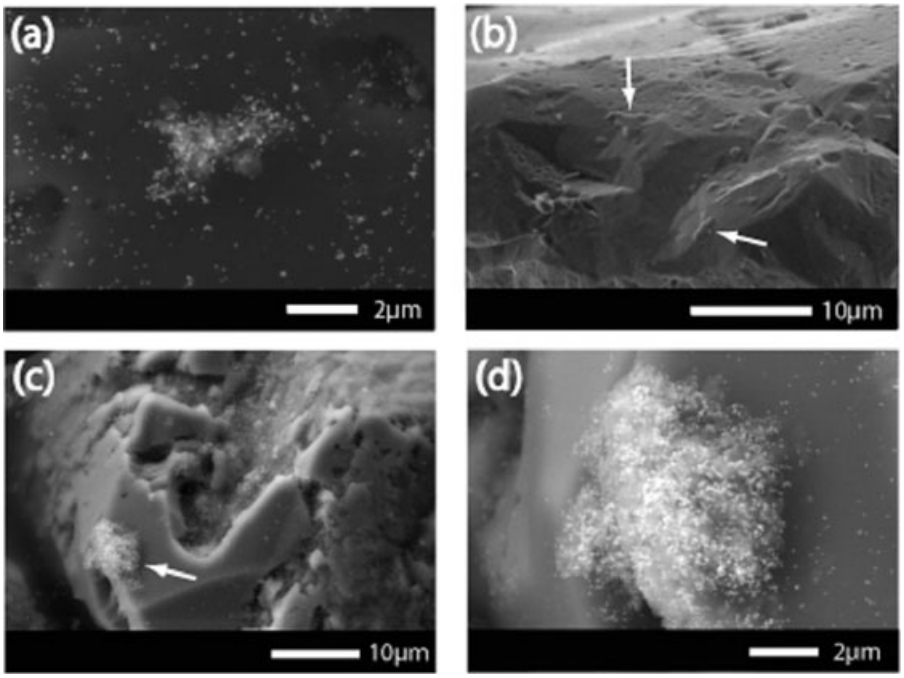

Fig. 3. *P. aeruginosa* cultures grown on quartz sand matrix. (a) Individual cells hybridized to nanogold probes appear as bright areas on quartz sand grain surfaces. In untreated cultures (b), *P. aeruginosa* often forms cell clusters (arrows in b) that are less visually distinct than the nanogold clusters observed on mineral surfaces in hybridized cultures (arrow in c, magnified image in d). Most of these larger (5–10 μm) nanogold clusters are localized in volatile coatings (seen in c and d) which presumably are biofilms.

the entire volume of the cell (Fig. 2), and the concentration of nanogold clusters varies somewhat (Fig. 2c-f). Unlike *E. coli* (Fig. 1), however, *P. aeruginosa* cells were carbon coated and were visualized under high vacuum with the ESEM to characterize nanogold particles with improved contrast and resolution. Surface textures and morphology of nanogold clusters are visible (Fig. 2f) as well as a faint cell envelope surrounding the hybridized gold particles (Fig. 2f and e). Because most of the biologic materials comprising the cell exterior for both *E. coli* and *P. aeruginosa* have been removed (presumably by Proteinase K permeabilization), nanogold clusters directly associated with the cell are visualized without backscattered electron imaging.

For hybridizations on PG201-sand cultures, nanogold-labelled cells were not as easily detected as with pure cultures. A few cell-shaped nanogold clusters were observed on sand grain surfaces (Fig. 3a) and appeared as larger aggregations associated with widespread biofilm-like colonies (Fig. 3c and d), rather than individual cell-shaped precipitates (seen in Figs 1 and 2). This biofilm-like texture is consistent with prior observations of unhybridized *P. aeruginosa* cell colonies on sand grain surfaces (Fig. 3b). The relative paucity of individual hybridized cells in the sand culture suggests that cell aggregates or biofilm substances are not completely removed during the permeabilization treatments. However, locations of rRNA-targeted nanogold hybridization are clearly identifiable by morphologically uniform, small (<150 nm) clusters of individual nanogold particles, indicating that hybridization can successfully target multi-cell aggregates or biofilm-like substances. Additional analytical techniques to locate gold in the sample (backscattered electron images) are not required.

In hybridization experiments where *Pyrococcus* was cultured in a matrix of elemental sulphur and pyrite particles, nanogold precipitates range from 20 nm to 10 μm in size (Fig. 4) and group into two different types: (1) multiple particles (<150 nm) clustered into aggregates ~2–8 μm in size (Fig. 4a–c) and (2) singular particles that are more angular in shape and ~2–10 μm in size (Fig. 4d–f). Both type (1) and type (2) gold precipitates are the same size as *Pyrococcus* cells (Jannasch *et al.*, 1992). However, rRNA hybridization with enhanced nanogold probes produces individual gold particles within the target cell in a uniform size range between 50 and 150 nm (Humbel *et al.*, 1995), similar to the type (1) aggregates. Furthermore, average variety values in Fig. 4(a), (b) and (c) range from 20 to 23, which is consistent with the values we obtained for rRNA nanogold probe binding in bacterial cells. This suggests that type (1) precipitates in Fig. 4(a)–(c) are hybridized *Pyrococcus* cells. The angular shapes, particle surface textures and average variety values of type (2) precipitates suggest that these are small pyrite and elemental sulphur grains which have nucleated nanogold precipitation during the hybridization experiment.

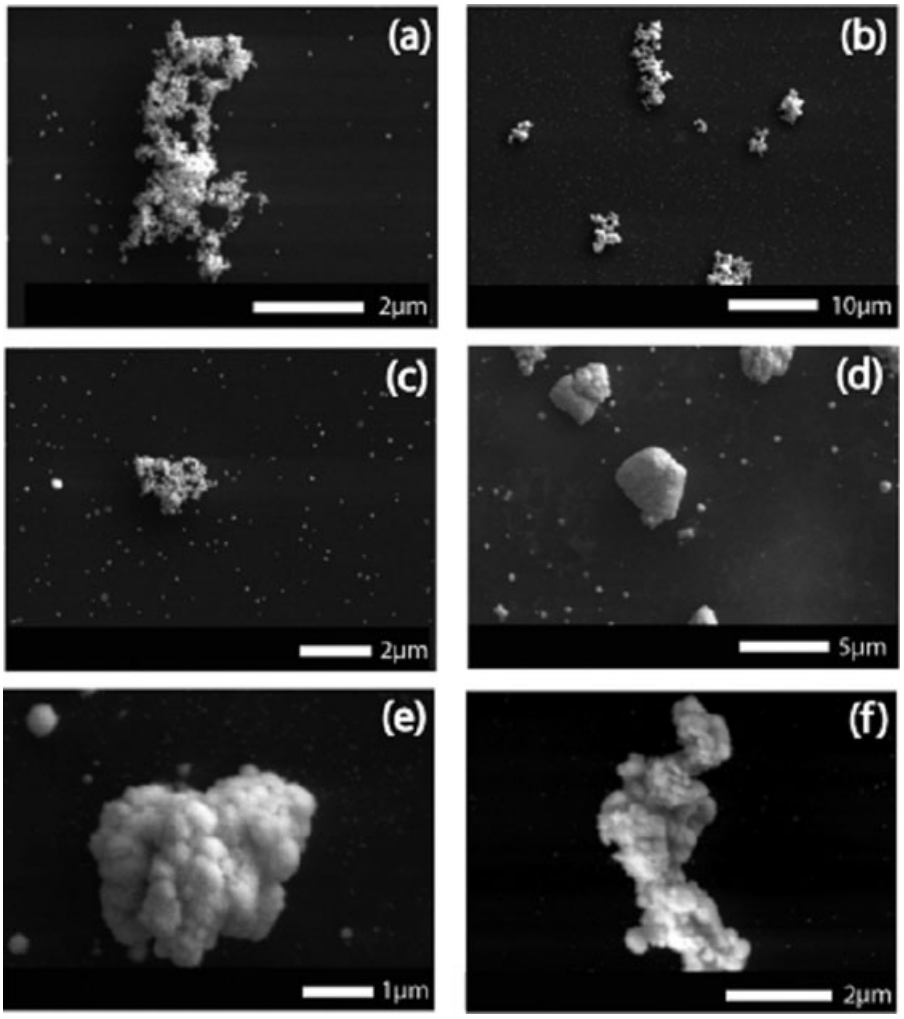

Fig. 4. Nanogold hybridizations with Pyrococcus cells grown with pyrite and elemental sulfur. Pyrococcus cells bound to Archaea-specific nanogold probes are shown in a, b and c. Mineral particles coated with nanogold are shown in d, e, and f. Cell specific binding seen in a, b, and c resulted in nanogold clusters composed of smaller (75–150 nm) particles arranged in the overall shape of Pyrococcus cells. Nonspecific precipitation of gold on mineral surfaces (shown in d, e, and f) shows different surface textures than rRNA-targeted nanogold binding. Surfaces of non–specific gold precipitate are smoother, and individual nanogold particles are not visible (see text). Cell-specific nanogold binding (a, b, c) exhibits variety values that are consistent with bacterial-specific nanogold hybridization (values between 20–23). Non–specific nanogold binding (d, e, f) exhibits lower average variety values ranging between 12–16.

The extensive non-specific precipitation of gold on mineral surfaces in this experiment underscores the importance and application of our technique to metal-rich environments. Because gold is homogeneously distributed on all surfaces throughout the sample, back-scattered electron imaging and energy dispersive X-ray spectroscopy microanalysis would not distinguish between rRNA-bound nanogold and gold precipitates on mineral surfaces. However, by removing the cell exterior and by examining morphological, textural and variety value differences between rRNA-targeted nanogold clusters and gold precipitation bound non-specifically to mineral surfaces, it is possible to identify hybridization events in these microbe-mineral systems.

Acknowledgements

This research was supported by National Science Foundation MRI, Ecology and Microbial Observatories programmes (MCB-0406999 and MCB-0534879, to RMH, PAH and SMS); the U.S. DOE NABIR programme; the U.S. EPA STAR programme. ESEM was performed in MEIAF (http://www.bren.ucsb.edu/facilities/MEIAF/) at UCSB by Jose Saleta (UCSB) and Randy Mielke (NASA-JPL).

References

Delong, E.F. (1992) Archaea in coastal marine environments. *Proc. Natl. Acad. Sci. U S A* **89**, 5685–5689.

Delong, E.F., Wickham, G.S. & Pace, N.R. (1989) Phylogenetic stains: ribosomal RNA-based probes for the identification of single microbial cells. *Science* **243**, 1360–1363.

Gerard, E., Guyot, F., Philippot, P. & Lopez-Garcia, P. (2005) Flourescence *in situ* hybridisation coupled to ultra small immunogold detection to identify prokaryotic cells using transmission and scanning electron microscopy. *J. Microbiol. Methods* **63**, 20–28.

Humbel, B.M., Sibon, O.C.M., Stierhof, Y.D. & Schwarz, H. (1995) Ultrasmall gold particles and silver enhancement as a detection system in immunolabeling and *in situ* hybridization experiments. *J. Histochem. Cytochem.* **43**, 735–737.

Jannasch, H.W., Wirsen, C.O., Molyneaux, S.J. & Langworthy, T.A. (1992) Comparative physiological studies on hyperthermophilic archaea isolated from deep-sea hot vents with emphasis on Pyrococcus strain GB-D. *Appl. Environ. Microbiol.* **58**, 3472–3481.

Kenzaka, T., Ishidoshiro, A., Yamaguchi, N., Tani, K. & Nasu, M. (2005) rRNA Sequence-based scanning electron microscopic detection of Bacteria. *Appl. Environ. Microbiol.* **71**, 5523–5531.

Menez, B., Rommevaux-Jestin, C., Salome, M., Wang, M., Philippot, P., Bonneville, A. & Gerard, E. (2007) Detection and phylogenetic identification of labeled prokaryotic cells on mineral surfaces using scanning X-ray microscopy. *Chem. Geol.* **240**, 182–192.

Priester, J.H., Horst, A.M., Van De Werfhorst, L.C., Saleta, J., Mertes, L.A.K. & Holden, P.A.H. (2007) Enhanced visualization of microbial biofilms by staining and environmental scanning electron microscopy. *J. Microbiol. Methods* **68**, 577–587.

Richards, R.G., Stiffanic, M., Owen, G.R.H., Riehle, M., Gwynn, A.P. & Curtis, A.S.G. (2001) Immunogold labeling of fibroblast focal adhesion sites visualized in fixed material using scanning electron microscopy. *Cell Biol. Int.* **25**, 1237–1249.

Weipoltshammer, K., Schofer, K., Almeder, M. & Wachtler, F. (2000) Signal enhancement at the electron microscopic level using Nanogold and gold-based autometallography. *Histochem. Cell Biol.* **114**, 489–495.

